Unfolding the Damping Behavior of Multilayer Graphene Membrane in the Low-Frequency Regime

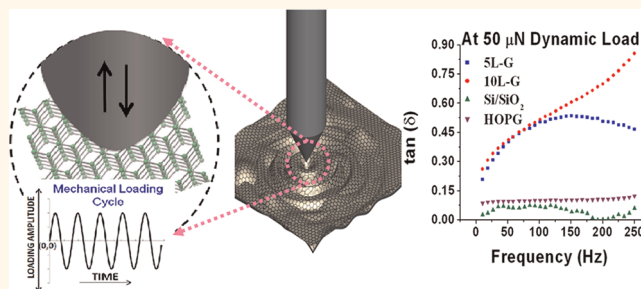Debrupa Lahiri,[†] Santanu Das,[‡] Wonbong Choi,[‡] and Arvind Agarwal[†],*

[†]Nanomechanics and Nanotribology Laboratory and [‡]Nanomaterials and Device Laboratory, Department of Mechanical and Materials Engineering, Florida International University, Miami, Florida 33174, United States

D amping characteristics of graphene are of paramount interest considering its numerous fields of applications such as nanomechanical resonators,[1−6] transparent electrodes,[7,8] heat spreaders,[9] nonvolatile memory,[10] thin film speakers,[11] acoustic emission devices,[12] and many more. The damping potential of graphene could also be very effective in macroscale dynamic systems, *e.g.*, tracking and pointing weapon systems in aircraft and suspension and steering in automotive and turbomachinery mountings, which need damping from shock vibrations.[13,14]

The experimental[1−6] and theoretical[15−17] studies performed on the damping/vibrational behavior of graphene, to date, are at a higher frequency range (>MHz), through electrostatic actuation. The theoretical studies on high-frequency regime vibrational behavior of single and multilayer suspended graphene have used molecular dynamics and continuum models to derive the vibration mode shapes, natural frequencies, and the influence of van der Waals interactions.[15−17] Bunch *et al.* established the application of graphene for nanomechanical resonators, in synergy with its excellent charge sensitivity.[1] Further experimental studies have explored the stress distribution on the graphene resonators,[2] their response to mass and temperature,[3] and the nonlinear damping behavior.[4] Low-frequency damping of graphene has a significant contribution toward graphene-based micro/nanoscale devices and macroscale dynamic systems for absorbing shock-generated energies.[13] *But the damping behavior of graphene in the low-frequency regime is not reported to date.*

In contrast to the available high-frequency damping studies, we have experimentally investigated the damping behavior of graphene at a much lower frequency (10−250 Hz) by application of cyclic mechanical load (0.1−50 μN). The aim of the present study is to comprehend the *low-frequency* damping behavior of graphene in light of the interplay between out-of-plane van der Waals and in-plane sp[2] bonds, which would govern the elastic and viscoelastic behavior of graphene in this regime. The role of cycling loading-assisted dynamicity of ripples in the energy absorption

ABSTRACT

The damping behavior of few-layered graphene membrane in the *low-frequency regime* of mechanical loading is investigated in the present study. Damping of graphene has significant applications in micro/nanoscale devices and macroscale dynamic systems for absorbing shock-generated energies. Damping behavior of graphene is experimentally evaluated, for the first time, by dynamic mechanical analysis at the nanoscale with cyclic mechanical loading in the range 0.1−50 μN applied at a frequency range of 10−250 Hz. This study reveals 260% higher damping on graphene membranes than a silicon surface. The damping shows excellent reproducibility and remains steady even after 100 000 cycles. The damping of multilayer graphene membrane, supported on a Si/SiO$_2$ substrate, shows a strong dependence on the frequency of cyclic loading. The mechanism governing impressive damping of a graphene membrane is elucidated by structural changes such as ripple formation, ripple wave propagation, and *z*-axis compression. Damping behavior of a graphene membrane in this low-frequency regime is also found to depend on the number of graphene layers and is explained as the interplay between in-plane sp^2 and out-of-plane van der Waals forces. These findings are important for establishing the potential of graphene for applications in macro- to nanoscale structures that require continuous absorption of shock waves without destruction/failure.

KEYWORDS: multilayer graphene · damping · dynamic ripple · nano-DMA · shock absorption · frequency · cyclic loading
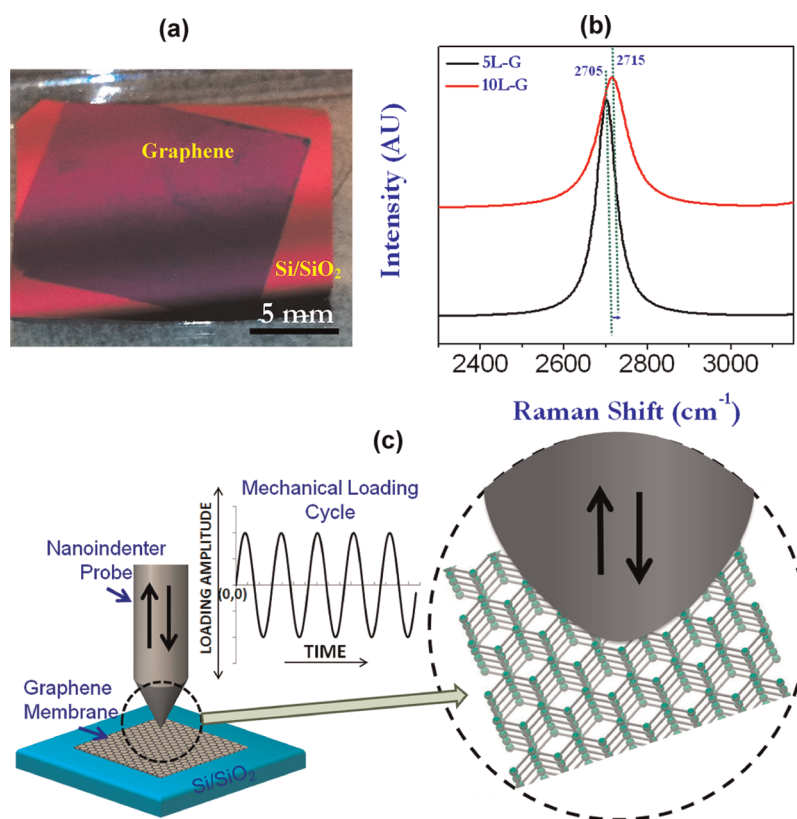
Figure 1. (a) Digital image of 5L-G on a Si/SiO$_2$ substrate. (b) Comparative Raman spectra of various layers of graphene on Si/SiO$_2$ substrates exhibiting the characteristic 2D band of graphene. (c) Schematic showing nano-DMA of the graphene membrane on a Si/SiO$_2$ substrate.

and its contribution toward the damping behavior of graphene membranes is also analyzed. This is the first experimental study on low-frequency damping behavior of graphene.

RESULTS AND DISCUSSION

The present study uses chemical vapor deposition (CVD)-grown graphene, which was transferred on a Si/SiO$_2$ substrate for studying the damping behavior. The transferred membrane consists of about 4 or 5 layers of graphene sheets, as observed in HRTEM (Figure S1, Supporting Information[18]), and is referred to as 5L-G, hereafter. Another sample was prepared by transferring a second membrane on top of another, thus consisting of 8–10 layers of graphene and is referred as 10L-G. It is expected that the second transferred layer of graphene could have some crystallographic misalignment with the first layer of graphene. The double transferred graphene membrane was annealed to reduce the interfacial mismatch and induce bonding between the two transferred membranes. Sample 5L-G was also given a similar annealing treatment after transferring onto the substrate.

The peak related to the 2D band in the Raman spectra for 5L-G and 10L-G provides additional support for relative graphene layer content in the two membranes (Figure 1b). The 2D peak in 5L-G is located at

$\sim$2705 cm^{-1}, which corresponds to $\sim$4 or 5 layers of graphene in the membrane.[19,20] A blue shift in the same peak to $\sim$2715 cm^{-1} indicates the presence of 8–10 layers in the 10L-G membrane.[19,20] A similar graphene membrane was also transferred on a Si/SiO$_2$ surface with a matrix of 50 μm diameter holes to study the existence of micrometer size dirt at the interface and top of the membrane. Transparent graphene membranes on a Si/SiO$_2$ substrate with comparable optical micrographs reveal a dirt-free surface of the membrane from micrometer-level impurities (Figure S2, Supporting Information). However, some atomic-scale impurities may be present at the interface of the wet transferred graphene membrane and the Si/SiO$_2$ substrate.

Damping behavior was evaluated through nanodynamic mechanical analysis (nano-DMA) in a frequency range of 10–250 Hz and dynamic (cyclic) load range of 0.1–50 μN (Figure 1c). Damping characteristics of the bare Si/SiO$_2$ surface is also determined to study the substrate effect. The damping of graphene is expressed as "tan (δ)", where δ is the phase lag between force applied and displacement obtained (see Supporting Information and Figure S3 for the measurement principle). Higher damping causes higher phase lag.

Both 5L-G and 10L-G show significant changes in the damping behavior with the frequency (Figure 2a and b).
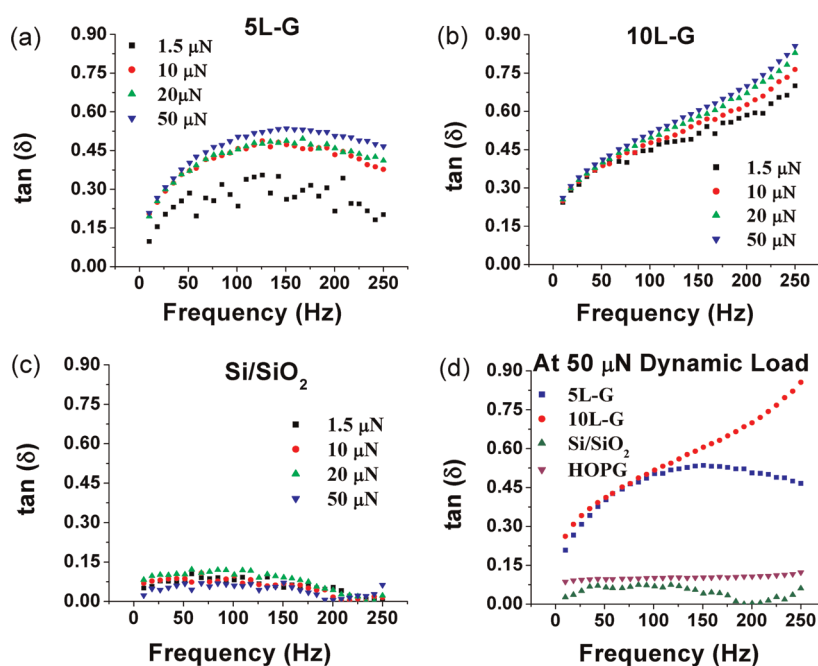
Figure 2. Damping behavior in the frequency range 10−250 Hz for (a) 5 L-graphene (b) 10 L-graphene, and (c) bare Si/SiO$_2$ at different dynamic load amplitudes. Si/SiO$_2$ substrate shows very low damping (<0.1) and almost no change with the frequency. (d) Comparative dynamic behavior of 5L-G, 10L-G, bare Si/SiO$_2$ substrate, and highly ordered pyrolytic graphite (HOPG) at a dynamic load of 50 μN and varying frequency.

Damping (tan δ) reaches a peak in 5L-G at ∼150 Hz and then decreases for loads between 1.5 and 50 μN (Figure 2a). On the contrary, damping continues to increase with the frequency for 10L-G up to 250 Hz (Figure 2b). Damping is similar in 5L-G and 10L-G up to ∼150 Hz (Figure 2d). The Si/SiO$_2$ substrate shows much lower tan δ (Figure 2c and d) and thus eliminates the possibility of contributing toward the damping response of both graphene membranes. Also, damping increases slightly at higher dynamic load (Figure 2a and b). These observations indicate a dominating influence of the frequency on the damping behavior. Similar observations are made in Figure 3, where increasing the dynamic load causes a slight increase in the damping for both graphene membranes at fixed frequencies of 100 and 200 Hz. Further, damping of 10L-G remains similar to 5L-G at 100 Hz, but increases by almost two times at 200 Hz for the entire range of dynamic load, which corroborates earlier observations in Figure 2d. Thus, graphene membranes are found to show similar trends in damping behavior irrespective of the testing conditions, *i.e.*, changing frequency or changing dynamic loads (Figure S4, Supporting Information, provides a graphical representation of additional results). Figures 3c and S4c show damping behavior of 5L-G, 10L-G, and the substrate after 100,000 loading cycles. Tan δ is consistent with small error bars, implying the steadiness of the damping during the long life-span. Damping is almost zero in the Si/SiO$_2$ substrate, whereas 5L-G and 10L-G show very high values of tan δ. Small error bars in Figure 3c also indicate no significant damage to graphene layers and

bonds in the membranes. These observations indicate that the damping behavior of graphene membranes is governed by fundamental structural and morphological aspects, which are discussed below.

The nature of dynamic mechanical loading is more suitably defined by the impact- and indentation-based deformation behavior of graphene[13,21−26] as compared to high-frequency resonance through electrical actuation.[1−6] Hence, the deformation mode of graphene during nano-DMA is a combination of impact and indentation loadings.

Graphene possess a very high in-plane Young's modulus of ∼1 TPa[21] due to strong sp^2 bonds. However, the layers of the graphene membrane are held together by weak van der Waals forces, which strongly influences its mechanical behavior.[27] Strong sp^2 bonding increases the probability of the elastic response due to in-plane mechanical loading. Thus the initial energy absorption in multilayer graphene membranes takes place in the out-of-plane direction, mainly through the following two mechanisms: (i) dynamic ripple formation in individual graphene layers and (ii) energy absorption through van der Waals bonds, working as nonlinear springs, and gradual reduction in interlayer spacing.

Role of Ripples in Damping. During dynamic loading, ripple formation becomes inevitable in the graphene layers,[13] some part of which could be recovered during unloading. However, the unrecovered part causes absorption of the energy and damping. He *et al.* have studied dynamic ripple formation in monolayer graphene due to impact and predicted energy absorption with the ripple wave propagation.[13] The decay in the
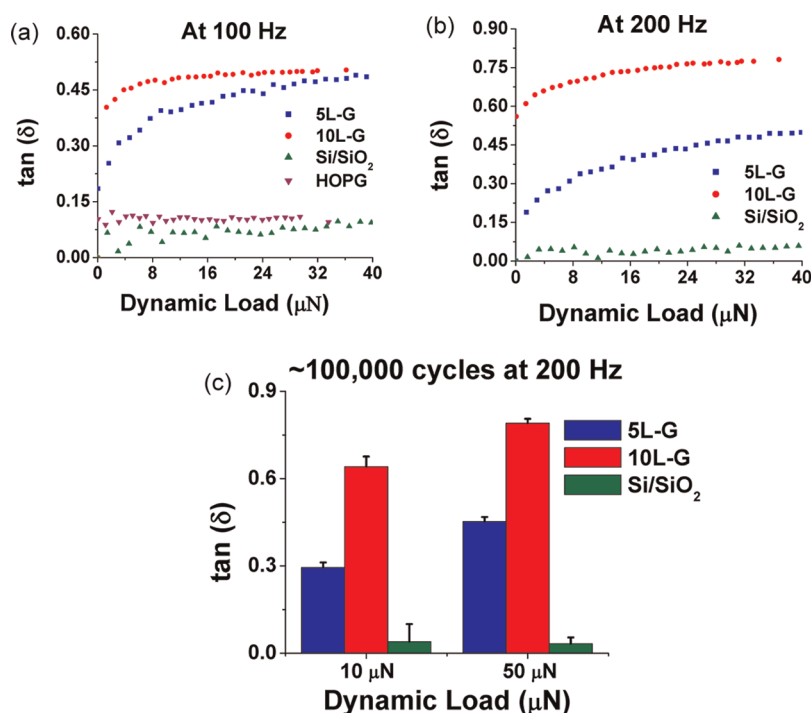
Figure 3. Comparative damping behavior of 5L-G, 10L-G, and Si/SiO$_2$ substrate at a dynamic load range of 0.1–40 μN with a frequency of loading of (a) 100 Hz and (b) 200 Hz. (c) Long cycle damping study for 5L-G, 10L-G, and Si/SiO$_2$ substrate at a frequency of 200 Hz and loads of 10 and 50 μN, showing the stability of the damping behavior of graphene membrane over 100,000 cycles of loading. 10L-G shows much higher damping than 5L-G, with almost negligible damping in Si/SiO$_2$.

amplitude of the ripple waves has been defined using the following relationship:

$$\text{amplitude}(x) = 2.59943 e^{(-|x|/7.33993)} - 0.01351 \quad (1)$$

where x is the horizontal distance of a ripple from the point of impact.[13] This relationship shows that ripple height is higher near the point of contact and decreases at a farther distance. It is emphasized that ripples that are intrinsic to graphene sheets[28] may lead to complex interactions with new ripples formed during loading. The ripples associated with the graphene membranes in this study are both intrinsic and originated from the transfer of graphene. These ripples might disturb the propagation of new ripple waves generated by the loading. However, theoretical study suggests that impacting ripple waves propagate forward and do not fade away completely.[13] Thus, dynamic wave formation due to the cyclic loading remains as one of the causes for the energy absorption in graphene membranes. Ripples can also play an active role in energy absorption during compressive loading. The flattening out of intrinsic ripples in the neighborhood of the stress/loading point[22] during nanoindentation of monolayer graphene is a potential cause for the damping. The force required for the flattening of ripples is much lower than in-plane stretching of graphene, which makes flattening more inevitable during loading of graphene layers with intrinsic ripples.[22] The schematic diagram in Figure 4 presents a graphical explanation of these two ripple-related energy absorption mechanisms.

van der Waals Contribution to Damping. Compressive deformation in graphene is initially dominated by out-of-plane weak van der Waals bonding, compared to strong in-plane sp^2 bonding. However, compression is restricted due to an increase in van der Waals force with decreasing interlayer distance. The van der Waals energy of interaction between two atoms 1 and 2 separated by distance H is defined as[29]

$$E = -\frac{\lambda_{1,2}}{H^6} \quad (2)$$

where $\lambda_{1,2}$ is London's constant, whose value depends on the atomic number. Hamaker modified the concept to quantify the van der Waals force between two spherical particles as[30]

$$F_{VDW} = \frac{AR}{12H^2} \quad (3)$$

where R is the reduced radius and A is Hamaker's coefficient, expressed as

$$R = \frac{2R_1 R_2}{R_1 + R_2} \text{ and } A = \pi q_1 q_2 \lambda_{1,2}$$

R_1 and R_2 are the radii of two particles; q_1 and q_2 are the atoms/cm^3 in the particles. The expression can be further modified for van der Waals force/unit area between two smooth plane surfaces (similar to graphene) as[29]

$$P_{VDW} = \frac{A}{6\pi H^3} \quad (4)$$

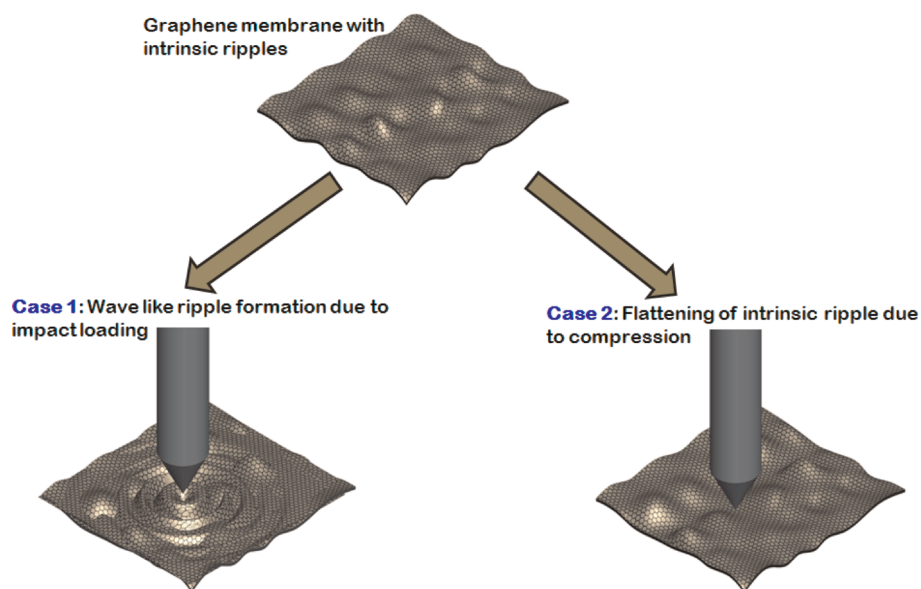Equation 4 shows an increase in the van der Waals force between two planes with a decrease in interplanar

Figure 4. Schematic showing the ripples in CVD-grown and transferred graphene and change in ripple structure with dynamic mechanical loading. The figure at the top shows a graphene membrane with ripples. Case 1 presents ripple wave propagation due to impact loading. The final ripple profile of the graphene membrane is the combined effect of the impacting waves and existing ripples, which are the primary cause of energy absorption. In case 2, the existing ripples are flattened due to the compressive loading. The flattening causes reduction in the amplitude of the existing ripples in the neighborhood of the indent in case 2, resulting in damping of the response to dynamic mechanical loading.

distance. This is the condition of graphene layers in a membrane during initial stages of compression. As the bonding between two layers becomes stronger with decreasing bond length (eq 4), it takes more energy to bring the two planes or particles closer or move them apart. In this process, the compressed membrane reaches a point when the force required to further compress the out-of-plane van der Waals bonds becomes higher than that for stretching the in-plane sp^2 bonds. From this point onward the deformation is dominated by sp^2 bonds. The energy absorption due to a decrease in interlayer distance of a multilayer graphene membrane is possible until the van der Waals force becomes very high and in-plane deformation (sp^2 dominated) starts taking place. During weak van der Waals domination, the nature of deformation remains viscoelastic with more damping. As sp^2 is a stronger bond, the associated deformation after transition is more elastic in nature, leading to a decrease in damping.

The damping increases with frequency up to ~150 Hz for both 5L-G and 10L-G (Figure 2). Increasing the frequency of loading causes more ripple formation and interlayer compression, because the graphene layers have less time to recover the ripples or deformation in the z-direction. This causes more absorption of energy and more damping. If the previous hypothesis holds true, then damping should continue to increase with the frequency. That is what we observe in the case of 10L-G in our experimental range of 10−250 Hz (Figure 2). However, for 5L-G, the damping decreases after ~150 Hz (Figure 2). The reason lies in the number

of graphene layers in the membrane. As postulated in eq 1, the ripple waves fade out in the x-direction along the propagation front. This means both 5L-G and 10L-G would have a similar spatial spread of the ripple propagation zone, but, due to more layer content in 10L-G, it can accommodate more ripple formation. Similarly, 10L-G has more space available along the z-axis to accommodate extra compression than 5L-G. At a frequency of loading higher than ~150 Hz, due to very fast ripple formation with less propagation time, the wavefront becomes saturated in the case of 5L-G. The situation is aggravated by less recovery in the z-direction due to faster loading cycles. So, the z distance between graphene layers is decreased enough to reach a transition point from van der Waals to sp^2 domination. Thus, the in-plane deformation starts to accommodate the cyclic load applied beyond 150 Hz. This leads to more elastic recovery and less damping in 5L-G above 150 Hz. In the case of 10L-G, more layers accommodate more ripple formation and more z-compression before reaching the transition, leaving less chance of in-plane C—C bond stretching. Thus, the damping increases beyond 150 Hz. It is possible that damping in 10L-G will start dying down at even higher frequency, when the critical z distance between graphene layers, corresponding to the deformation transition, is reached. However, it is also possible that at a very high frequency the damping behavior would be governed by some other phenomenon. Nano-DMA tests could not be carried out beyond 250 Hz due to limitation in machine capability. In addition to more ripple formation and z-axis compression, the possible
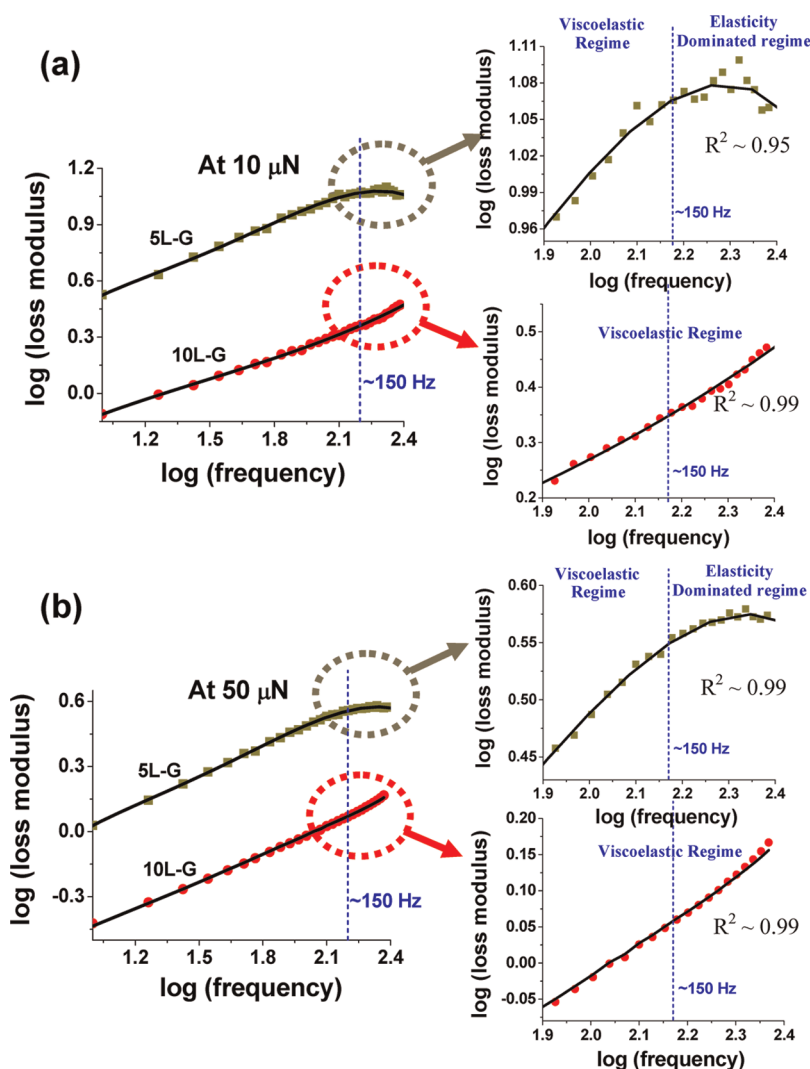
Figure 5. Log−log plot of frequency *vs* loss modulus for 5L-G and 10L-G at (a) 10 μN and (b) 50 μN dynamic loads. Polynomial fit is applied for a better visualization of the transition point. The polynomial fit shows a change in the slope for 5L-G at ∼150 Hz, denoting a viscoelastic to elastic transition in the deformation behavior. The absence of such slope change in 10L-G indicates no change in the damping mechanism in the experimental frequency range of 10−250 Hz.

interlayer crystallographic mismatch, caused during transfer, could assist in increased damping for 10L-G.

To ascertain the change in the deformation mechanism of 5L-G at ∼150 Hz, a log−log plot of loss modulus and frequency is obtained (Figure 5). This type of plot is commonly utilized for defining phase transformation in viscoelastic materials.[31] The sudden change in the slope for 5L-G at ∼150 Hz is similar in nature to the transition from rubbery to glassy regime in the case of polymers. At higher frequency, the dynamic deformation is supposed to be dominated by in-plane covalent bonding, making it more elastic (or less viscoelastic) in nature, which is similar to rubbery to glassy transition. On the contrary, 10L-G does not show any change in slope (and deformation behavior) throughout the frequency range.

Higher damping in 10L-G as compared to 5L-G raises the question of whether the damping on such structures would increase infinitely with the number of

graphene layers. To answer this query, a 1 mm thick highly oriented pyrolitic graphite (HOPG) sample was tested under some of the mechanical loading conditions used for graphene membranes. The results show much lower damping (tan $\delta \approx 0.1$) in HOPG than either of the graphene membranes (tan $\delta \approx 0.5$ and higher, Figures 2d and 3b). The reason for this behavior lies in the energy absorption by ripples in graphene membranes. HOPG, being a rigid 3D structure (no longer a complying membrane), does not have intrinsic ripples and is not prone to ripple formation. Thus, the energy absorption in HOPG is only through *z*-axis compression, and it exhibits lower damping than graphene membranes. In addition, the graphene layers of HOPG are stacked in perfect crystallographic alignment, unlike the crystallographic mismatch in transfer layers of 10L-G, as mentioned before. The perfect stacking of graphene layers in HOPG would also restrict the disturbance in structure by ripple formation to some

extent. This aspect has potential to contribute toward the difference in damping behavior between HOPG and 10L-G.

It is observed that dynamic load at fixed frequencies (Figure 3a and b) causes a smaller increase in the damping, compared to significant changes with an increasing frequency (Figure 2a and b) for both graphene membranes. The change in the load influences the z-axis compression, whereas change in the frequency is mainly accommodated through ripple formation. This understanding leads to the conclusion that the damping in graphene is more dominated by rippling than z-axis compression.

Long-cycle dynamic behavior also shows more damping for 10L-G than 5L-G at higher frequency (200 Hz), due to extended viscoelastic behavior of the former. SPM images of 5L-G after a long-cycle test reveals no residual impression of mechanical loading, indicating retention of the damage-free graphene structure (Figure S5, Supporting Information). Similar SPM images of Si/SiO$_2$ substrate after a long-cycle test indicate permanent deformation. This set of results provides encouraging input toward practical applications of graphene as a shock-resistant membrane for extended periods.

A brief nano-DMA study of a similar 5L-G graphene layer transferred on a single-crystal mica surface is also carried out to understand the universality of the damping behavior of graphene membranes. Mica is not the best substrate to reveal the full damping potential of graphene membranes because mica itself is known and used as a good vibration dampener.[32,33] The results, presented in Figure S6 (Supporting Information), show mica generating much higher damping (up to $\tan \delta \approx$ 0.4) than the Si/SiO$_2$ substrate ($\tan \delta \approx$ 0.1). However, it is more interesting to find out that graphene membranes can even enhance the damping capability (up to ~40%) of a surface like mica, which itself is known for its damping capabilities. However, the damping capability ($\tan \delta$) is found to decrease, both at higher frequency and at higher dynamic load, which is attributed to the damage of the mica substrate beneath the graphene membrane, causing permanent damage in the graphene membrane also. The signs of such damage can be observed in the SPM images in Figure S7, Supporting Information. The nano-DMA tests carried out on a graphene membrane over a mica substrate at 200 Hz frequency and 10 μN dynamic load for only 5000 cycles show signs of permanent damage, whereas no such features are observed on a graphene membrane over Si/SiO$_2$ even after 100,000 cycles of loading in similar conditions. The nature of change in $\tan \delta$ with frequency for a graphene—mica surface (Figure S6, Supporting Information) does not exactly match that for a graphene—Si/SiO$_2$ surface (Figure 2). The damping behavior of a graphene membrane on a mica surface is more influenced by the dampening from the substrate as compared to the rigid Si/SiO$_2$ substrate. Thus, damping behavior of a graphene membrane on a Si/SiO$_2$ substrate is more representative of the true behavior of graphene, whereas the different behavior on graphene—mica surface is attributed to the composite effect of substrate and membrane.

Excellent repeatability of the damping behavior of a graphene membrane on a Si/SiO$_2$ substrate, presented in Figure S8(a—c), Supporting Information, proves its intrinsic nature of origin. Atomic level impurities, if present at the graphene—Si/SiO$_2$ interface, do not show any significant contribution to the damping behavior. Otherwise, the damping behavior would be influenced in a localized manner and deviate from reproducibility, checked by a minimum of 50 tests in each membrane at a randomly selected spot with macroscale spatial distribution.

CONCLUSIONS

In summary, this study reveals excellent damping capability of few-nanometer graphene membranes in the low-frequency cyclic loading regime. The damping mechanism of the micrometer-level dirt-free graphene membrane is governed by structural changes such as ripple formation, ripple wave propagation, and z-axis compression. These results multiply the advantages of using graphene membranes in electronics and other nanoscale devices, as graphene membranes resist structural damage by mechanical impacts/shocks. This study paves the way for using graphene membranes as a nanoscale shock reservoir for impact-sensitive structures.

METHODS

Graphene Growth by CVD and Transfer to Si/SiO$_2$ Substrate. A copper foil of 54 μm thickness (NIMROD Hall, USA) was annealed at 1000 °C for 1 h in an argon atmosphere followed by surface cleaning with acetic acid at 70 °C. The preannealed metal foils were placed inside a 2 in. diameter quartz tube of a low-pressure thermal CVD system (Atomate, USA). Furnace temperature was raised to 1000 °C at a heating rate of 120 °C/min in an argon atmosphere. Graphene precipitation occurred on the Cu foil using the reaction of the precursor gas mixture of CH$_4$/H$_2$ (1:5) for 10 min. After the CVD process, the graphene film was transferred to a 300 nm SiO$_2$ coated Si substrate (Si/SiO$_2$) using a chemical process. The chemical process for graphene transfer consists of the etching of Cu foil and then transferring the floating graphene onto a Si/SiO$_2$ substrate, followed by washing with water, acetone, and isopropyl alcohol as described elsewhere.[18] Furthermore, the rapid thermal annealing was carried out for graphene on the Si/SiO$_2$ substrate at 400 °C under a N$_2$ atmosphere for 30—40 s. Similarly, the second graphene membrane was transferred onto the graphene—Si/SiO$_2$ substrate followed by annealing.

Raman spectroscopy of the graphene membranes was performed using a Spectra Physics (model 177G02) system with a spectral resolution of 4 cm^{-1} with an argon ion (Ar$^+$) laser

having a wavelength of 514.5 nm. The Raman spectra were collected using a high-throughput holographic imaging spectrograph (model HoloSpec f/1.8i, Kaiser Optical Systems) inbuilt with a volume transmission grating, a holographic notch filter, and a thermoelectrically cooled CCD detector (Andor Technology). Raman spectra were collected at room temperature and 1 atm.

Damping Characterization through nano-DMA Testing. Damping behavior of 5L-G, 10L-G, Si/SiO$_2$, and HOPG was characterized using the nano-DMA module of the Hysitron Triboindenter TI-900. For all the measurements, a 100 nm Berkovich diamond tip was used. The working principle of the nano-DMA module with the relevant equations is provided in the Supporting Information. The tests were performed with three different modes: (1) varying frequency with fixed load cycle; (2) varying load cycles with fixed frequency; (3) fixed load cycle and frequency with ~100 000 cycles of loading. During the tests, a cyclic dynamic load of 10% was applied over a fixed static load, with the indenter tip sitting on the sample surface. A minimum of 50 tests were carried out in each sample at macrolevel spatial distances randomly chosen on a >100 mm^2 surface area (Figure 1a) of each graphene membrane. Figure S8(a–c), Supporting Information, show the very high repeatability of the tests performed in some of these conditions.

Conflict of Interest: The authors declare no competing financial interest.

Supporting Information Available: HRTEM image of 5L-G, transfer procedure of free-standing graphene membrane on Si/SiO$_2$ with holes, optical images to evaluate cleanliness, calculation details for tan δ in the nano-DMA study, comparative damping behavior plots of 5L-G, 10L-G, and Si/SiO$_2$ (additional to those presented in the main text), scanning probe images of 5L-G and Si/SiO$_2$ surfaces after nano-DMA testing, damping behavior of mica and 5L-G on mica, comparative scanning probe images of graphene membrane on Si/SiO$_2$ and mica after long-cycle tests, three test data plots on graphene membranes in each condition to show the repeatability of the damping behavior. This material is available free of charge *via* the Internet at http://pubs.acs.org.

REFERENCES AND NOTES

1. Bunch, J. S.; van der Zande, A. M.; Verbridge, S. S.; Frank, I. W.; Tanenbaum, D. M.; Parpia, J. M.; Craighead, H. G.; McEuen, P. L. Electrochemical Resonators from Graphene Sheets. *Science* **2007**, *315*, 490–493.
2. Garcia-Sanchez, D.; van der Zande, A. M.; San Paulo, A.; Lassagne, B.; McEuen, P. L.; Bachtold, A. Imaging Mechanical Vibrations in Suspended Graphene Sheets. *Nano Lett.* **2008**, *8*, 1399–1403.
3. Chen, C.; Rosenblatt, S.; Bolotin, K. I.; Kalb, W.; Kim, P.; Kymissis, I.; Stormer, H. L.; Heinz, T. F.; Hone, J. Performance of Monolayer Graphene Nanomechanical Resonators with Electrical Readout. *Nat. Nanotechnol.* **2009**, *4*, 861–867.
4. Eichler, A.; Moser, J.; Chaste, J.; Zdrojek, M.; Wilson-Rae, I.; Bachtold, A. Nonlinear Damping in Mechanical Resonators Made from Carbon Nanotubes and Graphene. *Nat. Nanotechnol.* **2011**, *6*, 339–342.
5. van der Zande, A. M.; Barton, R.; Alden, J. S.; Ruis-Vargas, C. S.; Whitney, W. S.; Pham, P. H. Q.; Parpia, J. M.; Craighead, H. G.; McEuen, P. L. Large-Scale Array of Single-Layer Graphene Resonators. *Nano Lett.* **2010**, *10*, 4869–4873.
6. Barton, R. A.; Ilic, B.; vander Zande, A. M.; Whitney, W. S.; McEuen, P. L.; Parpia, J. M.; Craighead, H. G. High, Size-Dependant Quality Factor in an Array of Graphene Mechanical Resonators. *Nano Lett.* **2011**, *11*, 1232–1236.
7. Lii, X. S.; Zhu, Y. W.; Cai, W. W.; Borysiak, M.; Han, B. Y.; Chen, D.; Piner, R. D.; Colombo, L.; Rouff, R. S. Transfer of Large-Area Graphene Film for High-Performance Transparent Conductive Electrodes. *Nano Lett.* **2009**, *9*, 4359–4363.
8. Lahiri, I.; Verma, V. P.; Choi, W. An All-Graphene Based Transparent and Flexible Field Emission Device. *Carbon* **2011**, *49*, 1614–1619.
9. Prasher, R. Graphene Spreads the Heat. *Science* **2010**, *328*, 185–186.
10. Zheng, Y.; Ni, G. X.; Toh, C. T.; Zheng, M. G.; Chen, S. T.; Yao, K. Gate-Controlled Nonvolatile Graphene-Ferro-Electric Memory. *Appl. Phys. Lett.* **2009**, *94*, 163505.
11. Shin, K. Y.; Hong, J. Y.; Jang, J. Flexible and Transparent Graphene Films as Acoustic Actuator Electrodes Using Inkjet Printing. *Chem. Commun.* **2011**, *47*, 8527–8529.
12. Tian, H.; Ren, T.-L.; Xie, D.; Wang, Y.-F.; Zhou, C.-J.; Feng, T.-T.; Fu, D.; Yang, Y.; Peng, P.-G.; Wang, L.-G.; *et al.* Graphene-on-Paper Sound Source Devices. *ACS Nano* **2011**, *5*, 4878–4885.
13. He, Y. Z.; Li, H.; Si, P. C.; Li, Y. F.; Yu, H. Q.; Zhang, X. Q.; Ding, F.; Liew, K. M.; Liu, X. F. Dynamic Ripples in Single Layer Graphene. *Appl. Phys. Lett.* **2011**, *98*, 063101.
14. Koratkar, N.; Wei, B.; Ajayan, P. M. Carbon Nanotube Films for Damping Applications. *Adv. Mater.* **2002**, *14*, 997–1000.
15. He, X. Q.; Kitipornchai, S.; Liew, K. M. Resonance Analysis of Multilayer Graphene Sheets Used as Nanoscale Resonator. *Nanotechnology* **2005**, *16*, 2086–2091.
16. Kitipornchai, S.; He, X. Q.; Liew, K. M. Continuum Model for Vibration of Multilayered Graphene Sheets. *Phys. Rev. B* **2005**, *72*, 075443.
17. Iyakutti, K.; Surya, V. J.; Emelda, K.; Kawazoe, Y. Simulation of Single Later Graphene Sheets and Study of Their Vibrational and Elastic Properties. *Comput. Mater. Sci.* **2012**, *51*, 96–102.
18. Das, S.; Sudhagar, P.; Verma, V.; Song, D.; Ito, E.; Lee, S. Y.; Kang, Y. S.; Choi, W. Charge-Transfer Characteristics of Graphene for Triiodide Reduction in Dye-Sensitized Solar Cells. *Adv. Func. Mater.* **2011**, *2*, 3729–3736.
19. Rafiee, J.; Mi, X.; Gullapalli, H.; Thomas, A. V.; Yavari, F.; Shi, Y.; Ajayan, P. M.; Koratkar, N. A. Wetting Transparency of Graphene. *Nat. Mater.* **2012**, *11*, 217–222.
20. Ferrari, A. C.; Meyer, J. C.; Scardaci, V.; Casiraghi, C.; Lazzeri, M.; Mauri, F.; Piscanec, S.; Jiang, D.; Novoselov, K. S.; Roth, S.; *et al*. Raman Spectrum of Graphene and Graphene Layers. *Phys. Rev. Lett.* **2006**, *97*, 187401.
21. Lee, C.; Wei, X.; Kysar, J. W.; Hone, J. Measurement of the Elastic Properties and Intrinsic Strength of Monolayer Graphene. *Science* **2008**, *321*, 385–388.
22. Ruiz-Vargas, C. S.; Zhuang, H. L.; Huang, P. Y.; van der Zande, A. M.; Garg, S.; McEuen, P. L.; Muller, D. A.; Henning, R. G.; Park, J. Softened Elastic Response and Unzipping in Chemical Vapor Deposition Graphene Membranes. *Nano Lett.* **2011**, *11*, 2259–2263.
23. Huang, M.; Pascal, T. A.; Kim, H.; Goddard, W. A., III; Greer, J. R. Electronic-Mechanical Coupling in Graphene from *in-Situ* Indentation Experiments and Multiscale Simulations. *Nano Lett.* **2011**, *11*, 1241–1246.
24. Wang, C. Y.; Mylvaganam, K.; Zhang, L. C. Wrinkling of Monolayer Graphene: A Study by Molecular Dynamics and Continuum Plate Theory. *Phys. Rev. B* **2009**, *80*, 155445.
25. Frank, I. W.; Tanenbaum, D. M.; van der Zande, A. M.; McEuen, P. L. Mechanical Properties of Suspended Graphene Sheets. *J. Vac. Sci. Technol. B* **2007**, *25*, 2558–2561.
26. Poot, M.; van der Zant, H. S. J. Nanomechanical Properties of Few-Layer Graphene Membranes. *Appl. Phys. Lett.* **2008**, *92*, 063111.
27. Koenig, S. P.; Boddeti, N. G.; Dunn, M. L.; Bunch, J. S. Ultrastrong Adhesion of Graphene Membranes. *Nat. Nanotechnol.* **2011**, *6*, 543–546.

28. Fasolino, A.; Los, J. H.; Katsnelson, M. I. Intrinsic Ripples in Graphene. *Nat. Mater.* **2007**, *6*, 858–861.

29. London, F. The General Theory of Molecular Forces. *Trans. Faraday Soc.* **1937**, *33*, 8–26.

30. Hamaker, H. C. The London—van der Waals Attraction between Spherical Particles. *Physica* **1937**, *4*, 1058–1072.

31. Schoff, C. K. Molecular Organization and Dynamics: Rheological Measurements. In *Characterization and Analysis of Polymers*; John Wiley & Sons: Hoboken, NJ, 2008 (ISBN: 978-0-470-23300-9).

32. Basu, S.; Zhou, A.; Barsoum, M. W. On Spherical Nanoindentations, Kinking Nonlinear Elasticity of Mica Single Crystals and Their Geological Implications. *J. Struct. Geol.* **2009**, *31*, 791–801.

33. Deonath; Narayan, R.; Rohatgi, P. K. Damping Capacity, Resistivity, Thermal Expansion and Machinability of Aluminum Alloy-Mica Composites. *J. Mater. Sci.* **1981**, *16*, 3025–3032.